Macromolecules

ARTICLE

pubs.acs.org/Macromolecules

Effect of Photovoltaic Polymer/Fullerene Blend Composition Ratio on Microstructure Evolution during Film Solidification Investigated in Real Time by X-ray Diffraction

Monamie Sanyal, Benjamin Schmidt-Hansberg,* Michael F.G. Klein, Carmen Munuera, Alexei Vorobiev, Alexander Colsmann, Philip Scharfer, Uli Lemmer, Wilhelm Schabel, Helmut Dosch, and Esther Barrena*

Max Planck Institut für Metallforschung, Heisenbergstrasse 3, 70569 Stuttgart, Germany, Institut für Thermische Verfahrenstechnik, Thin Film Technology, Karlsruhe Institute of Technology, Kaiserstrasse 12, 76131 Karlsruhe, Germany, Lichttechnisches Institut, Karlsruhe Institute of Technology, Kaiserstrasse 12, 76131 Karlsruhe, Germany, European Synchrotron Radiation Facility, 6, rue Jules Horowitz BP220, 38043 Grenoble Cedex, France, Deutsches Elektronen-Synchrotron (DESY), Notkestr. 85, D-22607 Hamburg, Germany and Institut de Ciencia de Materials de Barcelona (ICMAB-CSIC), 08193 Bellaterra, Spain

ABSTRACT: We report an in situ X-ray investigation of the composition dependence on the structural evolution during drying of doctor-bladed blends of poly-(3-hexylthiophene) (P3HT) and [6,6]-phenyl C_{61}-butyric acid methyl ester (PCBM). This study enables an observation of the microstructure evolution in real time during blend crystallization. P3HT:PCBM blends with ratios of 1:0.5, 1:0.8, and 1:2 exhibit differing structural evolution during the course of solvent evaporation resulting in a different microstructure of the blends upon solidification. Large excess of PCBM over the eutectic composition impedes the $\pi-\pi$ packing of P3HT chains and leads to a not yet observed diffraction feature with an associated spacing of 12.6 Å, which might originate from a disordered phase of intimate mixed P3HT and PCBM molecules. This work provides a microscopic understanding of the composition dependence of the film formation from solution. The structural results are discussed in relation to the composition dependence of photovoltaic performance previously reported.

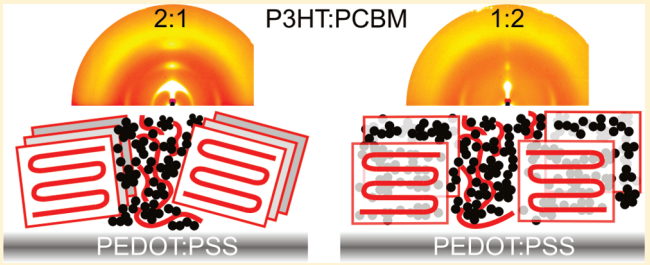

Organic photovoltaics are very promising as light-weight devices using solar energy for producing electricity - an important step toward increasing our utilization of renewable sources of energy. Of all organic photovoltaics, polymer solar cells (PSCs) are unrivalled in terms of processing cost, speed, and simplicity as the active materials can be solution-processed from most common organic solvents.[1−4] The substrates for PSCs range from flexible thin plastic films[5] to fibers and wires,[6,7] enabling them to be catered to myriad uses involving various device architectures. For high volume and large area production of PSCs, a continuous low-cost printing process like roll-to-roll (R2R) processing is required. In this respect, the process of doctor-blading, a coating technique whereby the active layer in solution is coated over the substrate with a knife edge, is well-suited. Although the performance of PSC is not as good as its inorganic counterparts, the situation is improving rapidly, and power conversion efficiencies of 8.3% have recently been reported.[8]

Most PSCs are based on the bulk heterojunction (BHJ) device structure where the photoactive film is fabricated by blending a polymeric electron donor with a fullerene-based electron acceptor in an organic solvent. In the final device the photoactive layer is sandwiched between two electrodes. The energy conversion involves two critical steps: the separation of photogenerated excitons to free charge carriers at the donor/acceptor interface and the efficient collection of the photogenerated charges at the electrodes. For a given combination of donor and acceptor materials, these two processes depend critically on the nanomorphology of the blend (e.g., molecular packing, crystallinity, spatial distribution, and size of the phase separated domains) that develops dynamically during its solidification. The nanomorphology of the dried film is strongly determined by the blending ratio and the material properties such as mutual miscibility, solubility, and surface energies.[9] The latter is especially important for the vertical gradient in P3HT-PCBM composition.[10−14] Still a major obstacle to enhance performance is the laborious empirical optimization of the blend composition and processing protocols. Hence, there is an imperious need of gaining knowledge about the phase behavior and crystallization of polymer/fullerene blends as a basis for a rational search of material combinations and fabrication methods.

The most widely studied BHJ consists of poly(3-hexylthiophene) (P3HT) and [6,6]-phenyl C_{61}-butyric acid methyl ester (PCBM). Devices made from this blend yield power conversion efficiencies over 4%[9,15−17] commonly due to improved nanomorphology achieved by slow drying[17−19] or upon thermal annealing.[20,21] Previous works have reported that the optimum P3HT:PCBM weight ratio composition for best device performance is close to 1:0.8.[22−28] This ratio dependence has recently

Received: January 7, 2011
Revised: March 29, 2011
Published: April 15, 2011

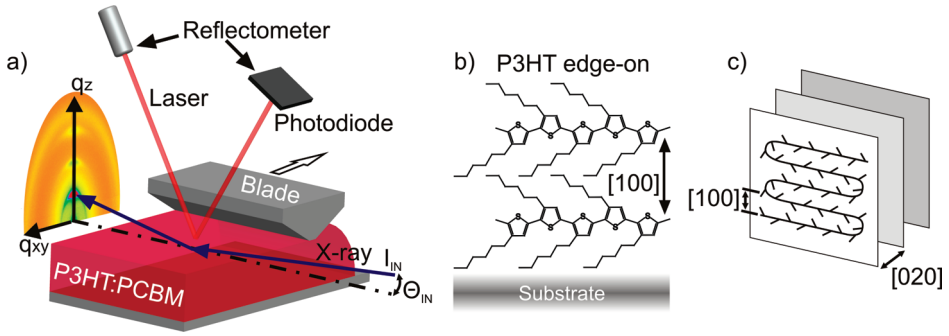

Figure 1. (a) Scheme of the experimental set up for simultaneous in situ grazing incidence X-ray scattering and optical reflectivity study of doctor-bladed P3HT:PCBM films during solvent evaporation. (b) Scheme of P3HT packing. For a predominantly edge-on orientation of P3HT crystallites, the P3HT interchain $\pi-\pi$ stacking lies in the sample plane, and hence the (100) and (020) reflections are observed along q_z and q_{xy}, respectively.

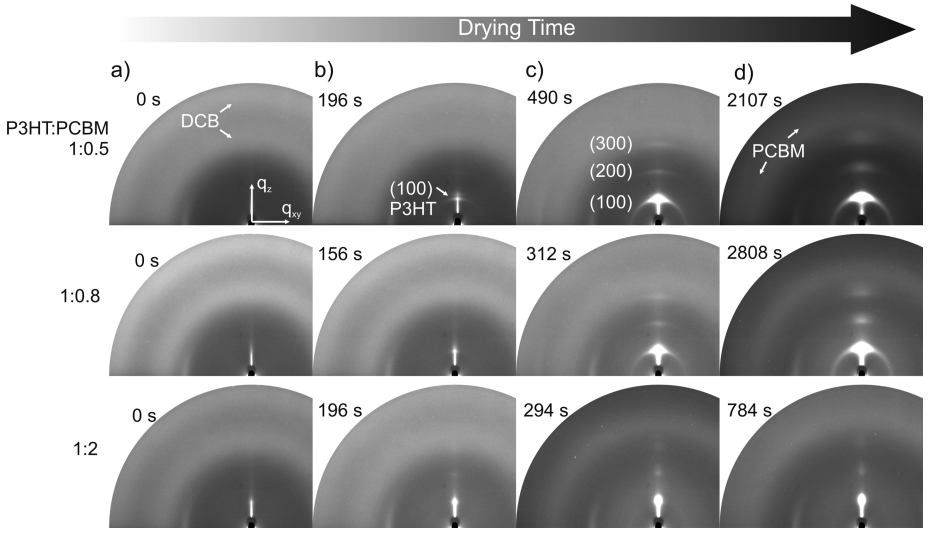

Figure 2. Two-dimensional X-ray diffraction patterns at different instants of evaporation of the solvent (DCB) for three blend ratios: (a) initial instant of drying, (b) first observation of the P3HT (100) peak, (c) observation of the P3HT (200) and (300), and (d) observation of PCBM diffraction ring. The time for complete film drying was ~500 s.

been explained by the eutectic phase behavior of binary organic blends, proposing that the optimum ratio is at a composition that is slightly hypoeutectic (i.e., with a slight excess of PCBM content).[25] It has been suggested that the nanomorphology at this hypoeutectic composition might favor a balanced transport of holes and electrons.[25,29] This work aims at providing further understanding of the composition dependence of the nanomorphology developing during blend crystallization in doctor-bladed films. The structural evolution during film drying is investigated by in situ X-ray diffraction for P3HT:PCBM blends with different blend ratios. This study enables the observation of blend crystallization as the solvent evaporates in real-time. We further perform an extended structural characterization of the dried films by combination of grazing incidence and specular X-ray diffraction. The different microstructures are discussed in the context of the ratio-dependent device properties reported in previous studies.

EXPERIMENTAL DETAILS

Film Preparation. Commercially available glass substrates were cleaned by sonication in acetone, followed by isopropanol for 10 min, respectively, and subsequently treated with oxygen plasma for 2 min. Poly(3,4-ethylenedioxythiophene):poly(styrenesulfonate) (PEDOT:PSS) dispersion (VPAI4083) was purchased from H.C. Starck. After sonication of the dispersion for 10 min, it was filtered (0.45 μm filter) and then diluted 1:1 by volume with demineralized water. The PEDOT:PSS layer was doctor-bladed on glass substrates (70 μm slit width and 5 mm/s coating speed). PEDOT:PSS enhances the photoinduced hole extraction on the anode interfacial layer and promotes planarization of the indium tin oxide surface. P3HT (molecular weight ~48 900 g/mol, polydispersity ~1.7, regioregularity of 90−94%) was purchased from Rieke Metals and PCBM was purchased from Solenne. P3HT and PCBM with weight ratios of 1:0.5, 1:0.8, and 1:2 were dissolved (3 wt % solid fraction) in *ortho*-dichlorobenzene (DCB) at 40 °C overnight (for ~15 h) and doctor-bladed with the same parameters as those for the PEDOT:PSS layer. For the real-time observation, slow drying conditions were applied (total time for film drying of ~500 s) by using a dedicated drying channel that was designed for providing accurate and reproducible drying conditions.[30,31] Without airflow, the ambient solvent vapor pressure increases and reduces the evaporation rate.

Method for Structure Characterization. For in situ characterization, a temperature-controlled drying channel with an integrated knife coater was built with lateral aluminum windows for X-ray scattering measurements and with a laser reflectometer on the top for film thickness measurement.[30] The initial thicknesses of the wet-coated films of P3HT:

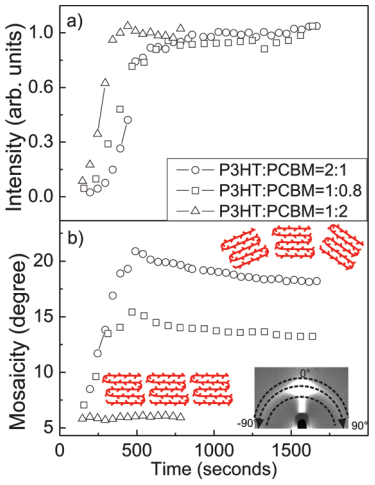

Figure 3. Evolution of (a) total integrated intensity of P3HT (100) Bragg peak and (b) mosaicity for blends with P3HT:PCBM ratios 1:0.5 (circles), 1:0.8 (rectangles), and 1:2 (triangles). The inset in the bottom right of part b shows the azimuthal integration of the first-order Bragg peak to calculate the mosaicity. The cartoons in part b show the lamellar orientation of P3HT for the different observed mosaicity.

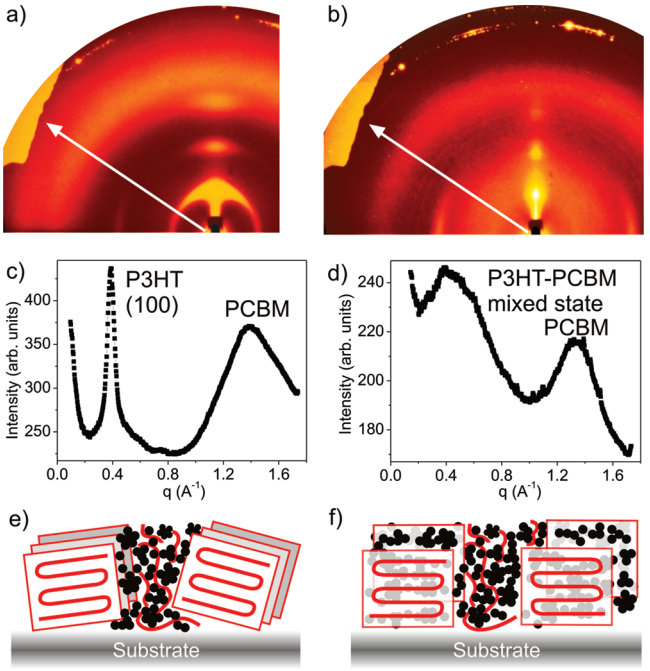

Figure 4. Two-dimensional diffraction pattern of dried blend films with P3HT:PCBM ratios of (a) 1:0.5 and (b) 1:2. Radial profiles (marked in the images) are shown in parts c and d. The diffraction ring corresponding to the P3HT: PCBM mixed structure, labeled in profile d, is observed for the blend with a P3HT:PCBM ratio of 1:2 at q = 0.498 Å^{-1}. The cartoon depicts the P3HT:PCBM blend structure in ratios of (e) 1:0.5 and (f) 1:2 on PEDOT:PSS-covered substrates.

PCBM blends with weight ratios of 1:0.5, 1:0.8, and 1:2, respectively, were 3850, 2730, and 2190 nm, resulting in dried films thicknesses of 200, 135, and 70 nm, respectively. Differences in the thickness of the coated blend solution due to the decreasing amount of higher viscous polymer are responsible for variations in the speed of drying.

In situ grazing incidence X-ray diffraction was carried out (wavelength λ = 0.934 Å) at the ID10B beamline in the European Synchrotron Radiation Facility (ESRF), Grenoble, France, using a 2D MAR-CCD detector. The 2D MAR-CCD images were corrected and translated into undistorted reciprocal space maps. As the solvent evaporated from the doctor-bladed wet film, 2D X-ray scattering patterns were taken for 3 s each in intervals of 50 s. The component q_z of the scattering vector **q** is defined as the component of **q** perpendicular to the sample surface (out-of-plane), whereas q_{xy} is along the sample surface (in-plane). The angle of grazing incidence was 0.135° for the 1:0.5 ratio, 0.125° for the 1:0.8 ratio, and 0.120° for the 1:2 ratio. At grazing incidence, the vertical axis in the 2D diffraction pattern does not represent the intensity of the true Bragg scattering along q_z but it contains a contribution of the in-plane component q_y. Therefore, dried films (with ratios 1:0.5 and 1:2 and for pure P3HT and PCBM films on technologically relevant glass/ITO/PEDOT:PSS substrates) were investigated by X-ray diffraction in detail using a point detector in the MPI-MF beamline of the synchrotron facility Ångströmquelle in Karlsruhe (ANKA). The energy used was 8 keV, and the incident angle was 0.175° (detector angle 0.35°).

RESULTS

The structural evolution of P3HT:PCBM dissolved in DCB was monitored by in situ GIXD instantly after doctor-blading the solution on a glass/PEDOT:PSS substrate for P3HT:PCBM in weight ratios of 1:0.5, 1:0.8, and 1:2 (Figure 1a). The thickness of the wet film was measured simultaneously by an optical reflectometer to have a direct correlation of the 2D diffraction patterns with the degree of drying.[30] Four 2D X-ray scattering frames are shown in Figure 2, illustrating different stages of drying for each of the investigated blend weight ratios. In the initial stages of drying, two broad diffraction rings were visible with associated spacing of 3.8 and 5.6 Å, which correspond to X-rays scattered from DCB (*a* in Figure 2). These diffraction rings progressively fainted in the course of solvent evaporation and disappeared completely when the solvent had evaporated. The observation of the first-order Bragg peak (100) in the early stage of drying was the first sign of P3HT crystallization (*b* in Figure 2). Soon, the second- and third-order diffraction peaks appeared (*c* in Figure 2). The average spacing of 16.5 Å associated with the (h00) peaks arises from the layered stacking of P3HT backbones separated by their hexyl side chains, adopting the so-called edge-on configuration (Figure 1b).[32−35] Toward the end of film drying, a broad diffraction ring becomes visible that is associated with PCBM aggregates randomly oriented in the blend (*d* in Figure 2). The described structural evolution occurs in a similar time scale for the three ratio compositions, although with a slight shift in the exact time due to differences in the thickness of the wet solvent-blend film doctor-bladed initially. (See the Experimental Details section.) A further detailed analysis of the structural evolution is presented in Figure 3. The crystallization process of P3HT can be estimated by quantifying the integrated X-ray intensity of the (100) Bragg peak as solvent evaporates. Note that this reflects the degree of P3HT ordering in a layered structure but not the quality of the P3HT interchain $\pi-\pi$ packing within the layers. The X-ray intensity was integrated between two concentric circles containing the (100) Bragg peak to account for the orientation distribution of P3HT crystallites, known as mosaicity and plotted as a function of drying time (Figure 3a and inset in Figure 3b). The integrated X-ray intensity plotted with respect to the azimuth angle has a Lorentzian distribution, whose full width at half-maximum (fwhm) gives a measure of the mosaicity. The plot shows the increase in P3HT (100) crystallinity, that is, layered lamellar ordering, that takes place until the evaporation of the solvent is complete (at ∼500 s).

dx.doi.org/10.1021/ma2000338 |*Macromolecules* 2011, 44, 3795–3800

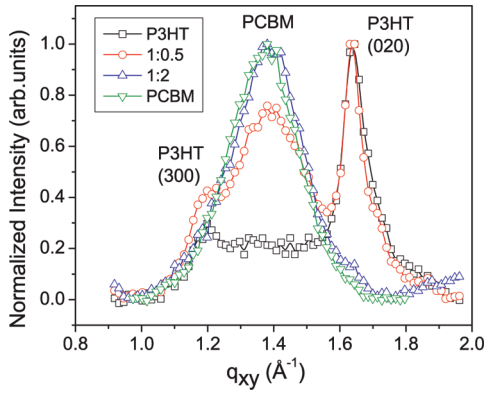

Figure 5. In-plane data obtained by GIXD using a point detector of films consisting of pure P3HT (black squares), P3HT:PCBM blend with 1:0.5 ratio (red circles), P3HT:PCBM blend with 1:2 ratio (blue triangles), and pure PCBM (green inverted triangles).

The impact of the blend ratio on the layer formation can be seen in the shape of the P3HT (h00) peaks (Figure 2). The larger mosaic spread of intensity observed for P3HT:PCBM ratios of 1:0.5 and of 1:0.8 reflects a relatively large orientation distribution of P3HT crystallites relative to the substrate plane. In contrast, the spot-like shape of the (h00) peaks for the 1:2 ratio indicates a stronger preference of edge-on orientation. Figure 3b shows the time evolution of mosaicity. The low mosaicity measured in the early stages of drying revealed a relatively narrow distribution of orientations for the three blend compositions. With drying time, the evolution was remarkably different for the blends with P3HT:PCBM ratios of 1:0.8 and 1:0.5, that is, for larger amount of P3HT. For these two compositions, the mosaicity increased considerably during the evaporation of the solvent to a maximum of 15.5° for the ratio of 1:0.8 and to 21° for the ratio 1:0.5 for the dried films. Beyond this time, a gradual decrease in mosaicity accompanied by a slight increase in crystallization occurs, which is attributed to slow reorganization of P3HT in the blend, most likely due to slow removal of remaining solvent molecules and interaction of remaining solvent in the channel (similar to solvent annealing effects).[11] For the blend with a ratio of 1:2, the situation is different as the mosaicity remained constant during the drying process. An additional structural feature was observed for this ratio: a broad diffraction ring with an associated spacing of 12.6 Å (Figure 4b,d). It is not a priori clear whether this diffraction ring originates from X-ray scattering of P3HT or PCBM molecules. We discard the hypothesis of it being a scattering feature of P3HT because the spacing observed differs considerably from the lattice spacing reported for crystalline[34−37] and disordered phases[34−37] of pure P3HT. Such spacing has not been reported for PCBM yet.[38−42] The center-to-center distance between neighboring PCBM molecules has been reported to be ∼10 Å.[38,39] However, it is worthwhile to mention that the crystalline structure of PCBM has not fully been characterized. Differences in experimental reported values suggest that the choice of solvent or crystallization conditions may affect the crystallization of PCBM.[38−42] Therefore, we cannot exclude that this broad scattering ring originates from amorphous PCBM formed for this blend ratio. There is still a third possibility to consider: the formation of a mixed structure consisting of the intercalation of PCBM molecules within the polythiophene backbones of P3HT, that is, breaking the P3HT $\pi-\pi$ stacking. This is schematically shown in Figure 4f along with the structural scheme for the blend with low PCBM content in Figure 4e but with P3HT interlayer $\pi-\pi$ stacking. The formation of disordered domains resulting from intimate mixing of P3HT and PCBM would agree with the large broadness of the diffraction ring, thereby indicating a short correlation length (calculated from the fwhm of the peak) and with the observed spacing of 12.6 Å. These issues will be further analyzed in the Discussion section.

Table 1. Correlation Lengths for P3HT $\pi-\pi$ Stacking and PCBM for the Different Blend Compositions

in-plane peak	P3HT	P3HT:PCBM 1:0.5	P3HT:PCBM 1:2	PCBM
P3HT (020)	86.9 Å	84 Å	absent	
PCBM		28 Å	32.5 Å	28.9 Å

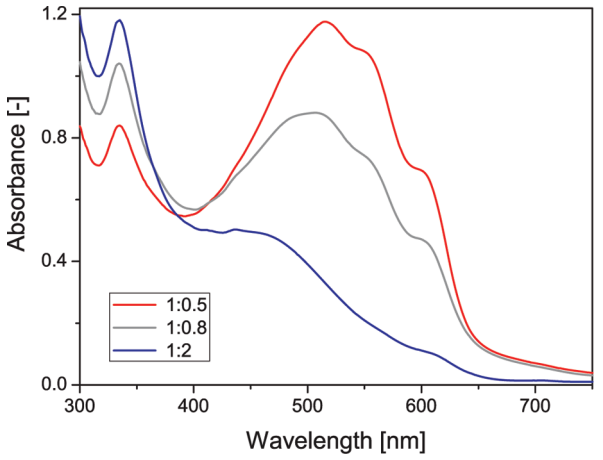

Figure 6. Absorption spectra of the at room-temperature doctor-bladed P3HT:PCBM films for different blending ratios.

Another structural issue of importance is the interlayer $\pi-\pi$ stacking of P3HT backbones because this is one of the crystalline directions of highest hole mobility.[44] Crystalline $\pi-\pi$ packing is associated with the (020) reflection (Figure 1b). In the 2D X-ray diffraction images, the (020) peak was observed only in the blends with P3HT:PCBM ratios 1:0.5 and 1:0.8. However, because signal-to-background ratio for the (020) peak was low, we performed additional GIXD measurements with a point detector. The in-plane scans are shown in Figure 5 for films of pure P3HT and PCBM and for blends with P3HT:PCBM ratios of 1:0.5 and 1:2. The (020) peak is observed only for the pure P3HT film, for the blend with 1:0.5, and for the blend 1:0.8 (not shown in Figure 5). The associated spacing of 3.8 Å is in agreement with previous reports.[42,45] The blending of P3HT with PCBM at this ratio does not influence significantly the correlation length of the $\pi-\pi$ stacking estimated from the full width at half-maximum (fwhm) of the (020) peak. The data confirms that the (020) peak is absent for the blend with highest PCBM content, that is, the 1:2 ratio, evidencing that PCBM hampers the development of interlayer $\pi-\pi$ stacking within the P3HT domains. No apparent differences are observed for the diffraction peak of PCBM, which shows a similar position (with an associated spacing of ∼4.5 Å) and width (coherence length of ∼30 Å for the pure and the blend films). The correlation length of the P3HT $\pi-\pi$ stacking and PCBM estimated from the fwhm of the P3HT (020) and PCBM peaks are listed in Table 1.

Additionally, absorption spectra (Figure 6) have been measured for the investigated blending ratios showing prominent vibronic shoulders at 560 and 605 nm for the 1:05 and 1:0.8 ratios associated with the $\pi-\pi$ stacking due to good interchain interaction. For the 1:2 ratio, the suppressed $\pi-\pi$ stacking of P3HT, which can be recognized by the disappearance of the vibronic shoulders, results in a strong overall blue shift of light absorption. In a previous work,[40] it could be shown that the height of the vibronic shoulders is correlated with the amount of $\pi-\pi$ stacked P3HT polymers, whereas the spacing and correlation length are not associated systematically.

DISCUSSION

We are going to discuss the observed structural differences in relation to previous studies regarding the ratio−dependence of the device properties. Optimum photocurrent generation is obtained from the optimum compromise between (i) high light absorption, achieved by maximizing the ordering of P3HT for a fixed thickness, (ii) efficient charge separation, realized by maximizing the donor−acceptor interface area, and (iii) balanced charge transport, accomplished by a balanced hole and electron transport and providing that both components form percolating paths toward the electrodes. Previous works reported that the optimum P3HT:PCBM ratio for best device performance is close to 1:0.8.[23−28] This has been explained by simultaneous increase in short−circuit current and fill factor, which are indeed drastically reduced with larger content of PCBM.[24,25,27,46,19] Optical UV−vis absorption studies showed that the spectral shape of pristine P3HT was preserved up to the 1:1 composition. For P3HT:PCBM ratios equal or larger than 1:2, a strong blue shift in the absorption was observed along with the disappearance of the two long−wavelength vibronic features, suggesting a disruption of the intermolecular P3HT $\pi-\pi$ packing for PCBM concentration larger than 50%.[46,19,47] Therefore, poor light harvesting at longer wavelengths and unbalanced charge transport were suggested as causes for reduction of short−circuit current. It has been shown that slowly spincast films, which are transferred in a wet state after spin-coating into a confined volume to allow slow drying of the solvent (solvent annealing), result in an optimized film morphology with higher power conversion efficiency.[17−19] We assume the slow-drying conditions of the doctor-bladed films here (Experimental Details section) to be comparable to the slow-drying conditions in spin-coated films because no external forces are applied to the drying film, as it is equally the case for doctor-bladed films. This is indeed suggested by the absorption spectra as a function of the PCBM content (Figure 6), which compare well with the results reported for slow-drying spin-coated films.[19]

The GIXD real-time study presented here reveals a remarkable effect of the PCBM content in the development and evolution of P3HT ordering during blend drying. It is found that the increase in PCBM content in the blend leads to a smaller angular distribution of P3HT crystallites, that is, with higher proportion of edge-on configuration. Interestingly, for the blend with highest PCBM content studied here, that is, of the P3HT:PCBM blend with ratio 1:2, the small angular distribution (mosaicity) of the initially nucleated P3HT crystallites remains constant during P3HT crystallization until the final film drying. This alignment effect favoring the edge-on orientation of P3HT with the increase in PCBM content is not well-understood. Presumably, the earlier solidification of PCBM crystals at this hypoeutectic composition limits the lateral growth of the initially nucleated P3HT crystallites, promoting its vertical growth. The larger percentage of edge-on crystallites is expected to be a hindering factor for charge carrier transport perpendicular to the substrate, as required for BHJ solar cells, given that the interlayer $\pi-\pi$ stacking direction is predominantly parallel to the surface.

Although for all blend compositions P3HT lamellae exhibit a layered structure (responsible for the observation of (h00) Bragg peaks in the out-of-plane direction), it is observed that PCBM hinders the development of P3HT interlayer $\pi-\pi$ stacking for the P3HT:PCBM blend with 1:2 ratio. This observation is thus in correlation with the disappearance of the two long wavelength features in the optical absorption spectra, as reported in the literature. Because the ordering of P3HT with $\pi-\pi$ stacking is considered an important structural factor for delocalization of charge carriers and polaron excitations over neighboring chains, the lack of $\pi-\pi$ packing is identified here as a cause for the observed poorer power conversion efficiency for 1:2 blends.

Finally, we retake the discussion of the broad diffraction ring observed for the 1:2 blend with an associated spacing of 12.6 Å. As commented before, this structural feature might be due to regions of pure PCBM in a disordered structure. Another reasonable hypothesis is the formation of a disordered mixed structure with PCBM intercalated between P3HT main-chain polythiophene polymer backbones, that is, along the sample surface in the q_{xy} direction. This would be consistent with the observed disruption of the P3HT interlayer $\pi-\pi$ packing for this composition, as revealed by GIXD and absorption spectra. In the case of intimate mixing of donor and acceptor at molecular level, charge recombination is expected to increase, reducing the overall conversion efficiency. An extended investigation of charge-transfer absorption in dependence with PCBM concentration would be necessary to give more insight into this issue.

CONCLUSIONS

In this work, it has been demonstrated that P3HT:PCBM blends with ratios 1:0.5, 1:0.8, and 1:2 exhibit a differing structural evolution during the course of solvent evaporation, resulting in a different microstructure of the blends upon solidification. Specifically, we have shown

(i) With increasing PCBM content, a larger portion of edge-on P3HT crystallites develop during drying.
(ii) Large excess of PCBM over the eutectic composition impedes the interlayer $\pi-\pi$ packing of P3HT chains, as proved here for the blend with P3HT:PCBM ratio of 1:2.
(iii) For the blend with P3HT:PCBM ratio of 1:2, a different diffraction feature emerges with an associated spacing of 12.6 Å, which might originate from a disordered phase of highly intermixed P3HT and PCBM molecules.

The differences in microstructure resulting for increasing PCBM content are expected to decrease light absorption and to contribute to a less efficient charge separation and transport. This work increases the microscopic understanding of the blend ratio-dependent film formation in relation to the structure−property relationships.

AUTHOR INFORMATION

Corresponding Author

*E-mail: schmidt-hansberg@kit.edu.; ebarrena@icmab.es.

■ ACKNOWLEDGMENT

The present work was funded by the German Research Foundation (Deutsche Forschungsgemeinschaft – DFG) within the priority program 1355 "Elementary processes of organic photovoltaics". We thank Ralf Weigel for his support in the MPI–MF beamline at ANKA, Mareike Kowalski, and Felix Buss. We acknowledge the European Synchrotron Radiation Facility for provision of synchrotron radiation facilities.

■ REFERENCES

(1) Young, M. N.; Huh, J.; Jo, W. H. *Sol. Energy Mater. Sol. Cells* **2010**, *94*, 1118–1124.
(2) Krebs, F. C.; Gevorgyan, S. A.; Alstrup, J. *J. Mater. Chem.* **2009**, *19*, 5445–5451.
(3) Krebs, F. C. *Sol. Energy Mater. Sol. Cells* **2009**, *19*, 5445–5451.
(4) Krebs, F. C. *Sol. Energy Mater. Sol. Cells* **2009**, *93*, 465–475.
(5) Gaudiana, R.; Brabec, C. J. *Nat. Photon* **2008**, *2*, 287–289.
(6) Fan, X.; Chu, Z.; Wang, F.; Zhang, C.; Chen, L.; Tang, Y.; Zou, D. *Adv. Mater.* **2008**, *20*, 592–595.
(7) O'Connor, B.; Pipe, K. P.; Shtein, M. *Appl. Phys. Lett.* **2008**, *92*, 193306–193308.
(8) Green, M. A.; Emery, K.; Hishikawa, Y.; Warta, W. *Prog. Photovoltaics: Res. Appl.* **2011**, *19*, 84–92.
(9) Peet, J.; Senatore, M. L.; Bazan, G. L. *Adv. Mater.* **2009**, *21*, 1521–1527.
(10) Germack, D. S.; Chan, C. K.; Hamadani, B. H.; Richter, L. J.; Fischer, D. A.; Gundlach, D. J.; DeLongchamp, D. M. *Appl. Phys. Lett.* **2009**, *94*, 233303–233305.
(11) Campoy-Quiles, M.; Ferenczi, T.; Agostinelli, T.; Etchegoin, P. G.; Kim, Y.; Anthopoulos, T. D.; Stavrinou, P. N.; Bradley, D. D. C.; Nelson, J. *Nat. Mater.* **2008**, *7*, 158–164.
(12) Xue, B.; Vaughan, B.; Poh, C.-H.; Burke, K. B.; Thomsen, L.; Stapleton, A.; Zhou, X.; Bryant, G. W.; Belcher, W.; Dastoor, P. C. *J. Phys. Chem. C* **2010**, *114*, 15797–15805.
(13) Huang, J.-H.; Chien, F.-C.; Chen, P.; Ho, K.-C.; Chu, C.-W. *Anal. Chem.* **2010**, *82*, 1669–1673.
(14) Beal, R. M.; Stavrinadis, A.; Warner, J. H.; Smith, J. M.; Assender, H. E.; Watt, A. A. R. *Macromolecules* **2010**, *43*, 2343–2348.
(15) Dennler, G.; Scharber, M. C.; Brabec, C. J. *Adv. Mater.* **2009**, *21*, 1323–1338.
(16) Ma, W.; Yang, C.; Gong, X.; Heeger, A. J. *Adv. Funct. Mater.* **2005**, *15*, 1617–1622.
(17) Li, G.; Shrotriya, V.; Huang, J.; Yao, Y.; Moriarty, T.; Emery, K.; Yang, Y. *Nat. Mater.* **2005**, *4*, 864–868.
(18) Mihailetchi, V. D.; Xie1, H.; de Boer, B.; Popescu, L. M.; Hummelen, J. C.; Blom, P. W. M.; Koster, L. J. A. *Appl. Phys. Lett.* **2006**, *89*, 012107–012109.
(19) Li, G.; Yao, Y.; Yang, H.; Shrotriya, V.; Yang, G.; Yang, Y. *Adv. Funct. Mater.* **2007**, *17*, 1636–1644.
(20) Shin, M.; Kim, H.; Park, J.; Nam, S.; Heo, K.; Ree, M.; Ha, C.-S.; Kim, Y. *Adv. Funct. Mat.* **2010**, *20*, 748–754.
(21) Agostinelli, T.; Lilliu, S.; Labram, J. G.; Campoy-Quiles, M.; Hampton, M.; Pires, E.; Rawle, J.; Bikondoa, O.; Bradley, D. D. C.; Anthopoulos, T. D.; Nelson, J.; Macdonald, J. E. *Adv. Funct. Mater.*, in press. DOI: 10.1002/adfm.201002076.
(22) Kim, J. Y.; Lee, K.; Coates, N. E.; Moses, D.; Nguyen, T.-Q.; Dante, M.; Heeger, A. J. *Science* **2007**, *317*, 222–225.
(23) Chirvase, D.; Parisi, J.; Hummelen, J. C.; Dyakonov, V. *Nanotechnology* **2007**, *15*, 1317.
(24) Kim, Y.; Choulis, S. A.; Nelson, J.; Bradley, D. D. C.; Cook, S.; Durrant, J. R. *Appl. Phys. Lett.* **2005**, *86*, 063502–063504.
(25) Mueller, C.; Ferenczi, T. A. M.; Campoy-Quiles, M.; Frost, J. M.; Bradley, D. D. C.; Smith, P.; Singelin-Stutzmann, N.; Nelson, J. *Adv. Mater.* **2008**, *20*, 3510–3515.
(26) Kim, J. Y.; Frisbie, C. D. *J. Phys. Chem. B* **2008**, *112*, 17726–17736.
(27) Van Bavel, S. S.; Baerenklau, M.; de With, G.; Hoppe, H.; Loos, J. *Adv. Funct. Mater.* **2010**, *20*, 1458–1463.
(28) Verploegen, E.; Mondal, R.; Bettinger, C. J.; Sok, S.; Toney, M. F.; Bao, Z. *Adv. Funct. Mater.* **2010**, *20*, 3519–3529.
(29) Baumann, A.; Lorrmann, J.; Deibel, C.; Dyakonov, V. *Appl. Phys. Lett.* **2008**, *93*, 252104–252106.
(30) Schmidt-Hansberg, B.; Klein, M. F. G.; Peters, K.; Buss, F.; Pfeifer, J.; Walheim, S.; Colsmann, A.; Lemmer, U.; Scharfer, P.; Schabel, W. *J. Appl. Phys.* **2009**, *106*, 124501.
(31) Schmidt-Hansberg, B.; Baunach, M.; Krenn, J.; Walheim, S.; Lemmer, U.; Scharfer, P.; Schabel, W. *Chem. Eng. Process.* **2011**. doi: 10.1016/j.cep.2010.12.012.
(32) Brinkmann, M.; Rannou, P. *Macromolecules* **2009**, *42*, 1125–1130.
(33) Winokur, M. J.; Spiegel, D.; Kim, Y.; Hotta, S.; Heeger, A. J. *Synth. Met.* **1989**, *28*, C419–C426.
(34) Prosa, T. J.; Winokur, M. J.; Moulton, J.; Smith, P.; Heeger, A. J. *Macromolecules* **1992**, *25*, 4364–4372.
(35) Tashiro, K.; Ono, K.; Minagawa, Y.; Kubayashi, M.; Kawai, T.; Yoshino, K. *J. Polym. Sci., Part B: Polym. Phys.* **1991**, *29*, 1223–1233.
(36) Pal, S.; Nandi, A. K. *Macromolecules* **2003**, *36*, 8426–8432.
(37) Mardalen, J.; Samuelsen, E. J. *Solid State Commun.* **1991**, *80*, 687–689.
(38) Rispens, M. T.; Meetsma, A.; Rittberger, R.; Brabec, C. J.; Sariciftci, N. S.; Hummelen, J. C. *Chem. Commun.* **2003**, *47*, 2116–2118.
(39) Yang, X.; Loos, J.; Veenstra, S. C.; Verhees, W. J. H.; Wienk, M. M.; Kroon, J. M.; Michels, M. A. J.; Janssen, R. A. J. *Nano Lett.* **2005**, *5*, 579–583.
(40) Sanyal, M.; Schmidt-Hansberg, B.; Klein, M. F.G.; Colsmann, A.; Munuera, C.; Vorobiev, A.; Lemmer, U.; Schabel, W.; Dosch, H.; Barrena, E. *Adv. Energy Mater.* **2011**, DOI: 10.1002/aenm.201100007.
(41) Kim, Y.; Cook, S.; Tuladhar, S. M.; Choulis, S. A.; Nelson, J.; Durrant, J. R.; Bradley, D. D. C.; Giles, M.; McCulloch, I.; Ha, C.-S.; Ree, M. *Nat. Mater.* **2006**, *5*, 197–203.
(42) Kim, J. Y.; Frisbie, C. D. *J. Phys. Chem. B* **2008**, *112*, 17726–17736.
(43) Napoles-Duarte, J. M.; Reyes-Reyes, M.; Ricardo-Chavez, J. L.; Garibay-Alonso, R.; Lopez-Sandoval, R. *Phys. Rev. B* **2008**, *78*, 035425–035431.
(44) Sirringhaus, H.; Brown, P. J.; Friend, R. H.; Nielsen, M. M.; Bechgaard, K.; Langeveld-Voss, B. M. W.; Spiering, A. J. H.; Janssen, R. A. J.; Meijer, E. W.; Herwig, P.; de Leeuw, D. M. *Nature* **1999**, 685–688.
(45) Kline, R. J.; McGhee, M. D.; Toney, M. F. *Nat. Mater.* **2006**, *5*, 222–228.
(46) Kim, Y.; Cook, S.; Choulis, S. A.; Nelson, J.; Durrant, J. R.; Bradley, D. D. C. *Chem. Mater.* **2004**, *16*, 4812–4818.
(47) Vanlaeke, P.; Swinnen, A.; Haeldermanns, I.; Vanhoyland, G.; Aernouts, T.; Cheyns, D.; Deibel, C.; D'Haen, J.; Heremans, P.; Poortmans, J.; Manca, J. V. *Sol. Energy Mater. Sol. Cells* **2006**, *90*, 2150–2158.
(48) Vandewal, K.; Gadisa, A.; Oosterbaan, W. D.; Bertho, S.; Banishoeib, F.; van Severen, I.; Lutsen, L.; Cleij, T. J.; Vanderzande, D.; Manca, J. V. *Adv. Funct. Mater.* **2008**, *18*, 2064–2070.
(49) Veldman, D.; Meskers, S. C. J.; Janssen, R. A. J. *Adv. Funct. Mater.* **2009**, *19*, 1939–1948.
(50) Hallermann, M.; Kriegel, I.; da Como, E.; Berger, J. M.; von Hauff, E.; Feldmann, J. *Adv. Funct. Mater.* **2009**, *19*, 3662–3668.